

Proteome-wide identification of poly(ADP-ribose) binding proteins and poly(ADP-ribose)-associated protein complexes

Jean-Philippe Gagné^{1,2}, Maxim Isabelle¹, Ken Sin Lo³, Sylvie Bourassa³, Michael J. Hendzel⁴, Valina L. Dawson⁵, Ted M. Dawson⁵ and Guy G. Poirier^{1,3,*}

¹Laval University Medical Research Center, CHUQ, Faculty of Medicine, Laval University, Québec, Canada G1V4G2, ²CNRS, UMR 6061, Institut de Génétique et Développement de Rennes, Université de Rennes 1, Rennes, France, ³Proteomics Platform, Québec Genomic Center, Laval University Medical Research Center, CHUQ, Faculty of Medicine, Laval University, Québec, Canada G1V4G2, ⁴Department of Oncology, University of Alberta and Cross Cancer Institute, Edmonton, Alberta, Canada T6G 1Z2 and ⁵Neuroregeneration and Stem Cell Programs, Institute for Cell Engineering, Department of Neurology and the Solomon H Snyder Department of Neuroscience, Johns Hopkins University School of Medicine, Baltimore, MD 21205, USA

Received July 17, 2008; Revised October 6, 2008; Accepted October 7, 2008

ABSTRACT

Poly(ADP-ribose) (pADPr) is a polymer assembled from the enzymatic polymerization of the ADP-ribosyl moiety of NAD by poly(ADP-ribose) polymerases (PARPs). The dynamic turnover of pADPr within the cell is essential for a number of cellular processes including progression through the cell cycle, DNA repair and the maintenance of genomic integrity, and apoptosis. In spite of the considerable advances in the knowledge of the physiological conditions modulated by poly(ADP-ribosyl)ation reactions, and notwithstanding the fact that pADPr can play a role of mediator in a wide spectrum of biological processes, few pADPr binding proteins have been identified so far. In this study, refined *in silico* prediction of pADPr binding proteins and large-scale mass spectrometry-based proteome analysis of pADPr binding proteins were used to establish a comprehensive repertoire of pADPr-associated proteins. Visualization and modeling of these pADPr-associated proteins in networks not only reflect the widespread involvement of poly(ADP-ribosyl)ation in several pathways but also identify protein targets that could shed new light on the regulatory functions of pADPr in normal physiological conditions as well as after exposure to genotoxic stimuli.

INTRODUCTION

The activation of poly(ADP-ribose) polymerases (PARPs) has been the subject of numerous studies in which poly(ADP-ribose) (pADPr), a branched polymer assembled upon the catalytic transfer of ADP-ribose moieties from NAD, was initially regarded as a posttranslational modification. Indeed, the covalent attachment of pADPr chains to chromatin-associated proteins, such as histones has been known for decades (1). Since then, a growing body of work on pADPr metabolism across a broad range of model systems has identified new pADPr-associated proteins. Whether these proteins are covalently poly(ADP-ribosyl)ated, noncovalent pADPr binding proteins or exhibiting both properties, they can collectively be termed pADPr-associated proteins. The methods used so far to identify pADPr-associated proteins are summarized in Figure 1. Current strategies include various biochemical and biological validation approaches, bioinformatics analysis for the prediction of pADPr binding motifs or *in vivo* cell imaging. In spite of the increasing number of tools currently used to identify pADPr-associated proteins, very little literature addresses the question of poly(ADP-ribosyl)ation from a pADPr binding perspective. Until recently, most of the attention to pADPr-associated proteins has been focused on covalent poly(ADP-ribosyl)ation because of the drastic consequences generally observed on protein properties (2). However, several studies are now pointing to important noncovalent interactions between pADPr and various

*To whom correspondence should be addressed. Tel: +1 418 654 2267; Fax: +1 418 654 2159; Email: guy.poirier@crchul.ulaval.ca

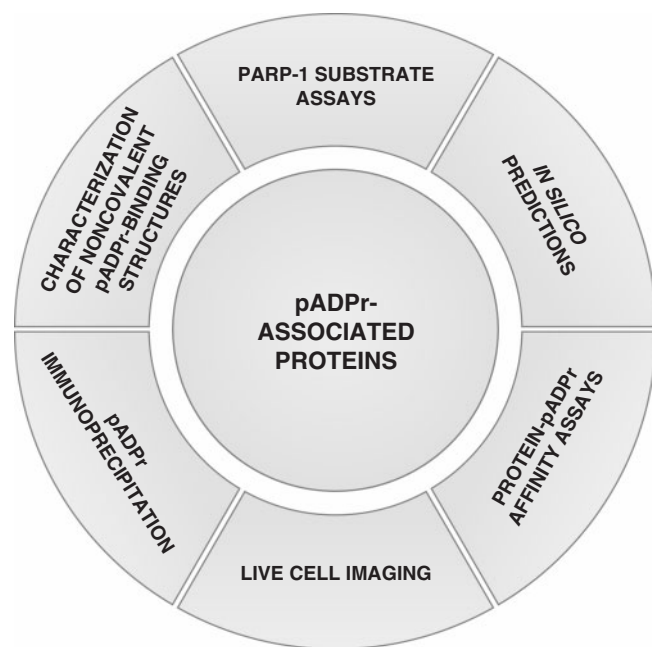


Figure 1. Current experimental strategies for the identification of pADPr-associated proteins. Six types of experimental approaches have been used to date to identify poly(ADP-ribose)ated and pADPr binding proteins (pADPr-associated proteins). As illustrated clockwise starting from the top: (i) identification of *in vitro* and *in vivo* poly(ADP-ribose) transferase activity of PARP-1 onto acceptor proteins (covalent modifications) using immunological or radioactivity-based detection methods; (ii) identification of noncovalent pADPr binding regions within protein amino acid sequences based on similarity with a consensus pADPr binding motif; (iii) affinity-based assays for the identification, validation and quantitative evaluation of noncovalent pADPr binding [surface plasmon resonance (SPR), electrophoretic mobility shift assays (EMSA), peptide and protein polymer blot analysis, mono- and bidimensional gel electrophoresis coupled with polymer blot analysis followed by MS]; (iv) *in vivo* evaluation of recruitment and accumulation of pADPr binding proteins using micro irradiation-induced DNA damage assays in live cell experiments; (v) immunoprecipitation assays using specific anti-pADPr antibodies to pull-down pADPr-associated proteins; and (vi) the characterization of PARP-associated protein domains as functional noncovalent pADPr binding modules (e.g. the Macro domain Alpp or the zinc-finger domain PBZ).

signaling proteins and an expanding number of proteins are now known to bind in a noncovalent manner to pADPr.

Three protein motifs have been characterized to mediate noncovalent pADPr binding. Pleschke *et al.* (3) were the first to report a noncovalent pADPr binding motif in DNA damage checkpoint proteins. This characteristic pADPr binding motif, composed of interspersed basic and hydrophobic amino acid residues, suggested for the first time that pADPr can act as a mediator of protein–protein interactions. A second pADPr binding motif has been shown by Karras and colleagues (4) to reside within macro domains in the form of a conserved ligand binding pocket (5). The pADPr binding of macro domain-containing proteins is particularly interesting given that this module is mostly found in helicase proteins associated with DNA and/or RNA unwinding activity, an important function in DNA replication, DNA repair and DNA recombination processes. A recent study from Ahel and colleagues

(6) has revealed a third structure (zinc-finger PBZ) found in DNA repair and checkpoint proteins, which also mediates specific pADPr binding.

These noncovalent pADPr motifs can be the object of pADPr-affinity evaluation. Indeed, Fahrner and colleagues (7) have published a quantitative method to assess the binding affinity of noncovalent pADPr binding proteins. They reported remarkably high noncovalent affinity to pADPr, this affinity being correlated to pADPr chain length, in consistency with the length-dependent behavior of pADPr in cell death (8), and the nanomolar affinity of macro domains.

Although some proteins bind pADPr through either a covalent or noncovalent bond, some proteins closely associated to PARPs may actually be modified by both mechanisms. Evidence is mounting that pADPr's functions extend far beyond that of a covalent posttranslational modification. pADPr can indeed be viewed as an effector molecule that modulate the properties of its acceptor proteins.

In view of the scarcity of information presently available and the potentially large number of pADPr-associated proteins, we conducted a proteome-wide investigation to identify candidates for pADPr binding and to determine if diversity exists in the roles of pADPr in cell function. First, *in silico* identification of consensus pADPr binding motifs was used to systematically identify putative pADPr binding proteins amongst a nonredundant human protein database. Second, synthetic peptides derived from the sequences of selected proteins that contained motifs with high homology to the predicted pADPr consensus binding site were tested for *in vitro* binding to pADPr. Positive binding sequences were aligned to refine the consensus pADPr binding motif into a more stringent pattern for increased confidence in pADPr binding predictions. Finally, *in silico* predictions were supported by protein–pADPr affinity assays coupled with large-scale mass spectrometry (MS)-based proteome analysis. Polymer blot analysis of two-dimensionally separated HeLa cell extracts revealed several proteins that were predicted to bind pADPr as well as pADPr-associated proteins identified by liquid-chromatography tandem MS (LC-MS/MS) that were immunoprecipitated from cell cultures exposed to extensive alkylation-induced DNA damage. Identified protein candidates were classified according to biological functions and their known interactions with pathways-related proteins so as to organize them into biologically meaningful clusters. Collectively, our results provide novel insights into the pADPr interactome and generate, for the first time, a large-scale MS-based proteomic resource for identifying pADPr binding candidates.

MATERIALS AND METHODS

In silico prediction of pADPr binding proteins

Putative pADPr binding proteins were first screened on the basis of the original consensus pADPr binding motif proposed by Pleschke *et al.* (3). The following original pattern value [AVILMFYW]₁-X₂-[KR]₃-X₄-[AVILMFY]₅-[AVILMFYW]₆-[KR]₇-[KR]₈-[AVILMFYW]₉-[AVI

LMFYW]₁₀-[KR]₁₁ was searched against the *Homo sapiens* entries of the Swiss-Prot database (20 070 human entries out of 392 667, as indexed on 23 July 2008) using the PattInProt search engine located on the NPS@ server (Network Protein Sequence @analysis, <http://npsa-pbil.ibcp.fr/>) (9). A similarity level cut-off of 90% was applied. The refined pADPr binding motif [HKR]₁-X₂-X₃-[AIQVY]₄-[KR]₅-[KR]₆-[AILV]₇-[FILPV]₈ was screened using the same database but without mismatch (100% similarity).

Cell culture, siRNA transfections and induction of DNA damage

Human neuroblastoma SK-N-SH and HeLa cervical carcinoma cell lines were cultured (air/CO₂, 19:1, 37°C) in DMEM medium supplemented with 10% fetal bovine serum (Hyclone-ThermoFisher Scientific, Ottawa, Canada). Penicillin (100 U/ml) and streptomycin (100 mg/ml) (Wisent, St-Bruno, Canada) were added to culture media. When growth of SK-N-SH cells reached ~50% confluency, cells were transfected with 5 nM PARG siRNA [hPARG: AAGAUGAGAAUGGUGAGCGAA dTdT and hPARG control siRNA (mismatch): AAGAUGAGAAUCCUGAGCGAA dTdT] using HiPerfect reagent (Qiagen, Mississauga, Canada). Silencing was conducted over 6 days, passaging cells every 48 h to achieve maximum PARG knockdown. Alkylating DNA damage was performed using 100 µM *N*-methyl-*N'*-nitro-*N*-nitrosoguanidine (MNNG) for 5 min.

Two-dimensional polymer blot analysis

Five hundred micrograms of total HeLa cell protein extracts were subjected to high-resolution two-dimensional electrophoresis essentially following the method developed by O'Farrell (10). Briefly, cells were lysed in a lysis buffer containing 9 M urea, 2% NP-40 and 2% ampholines (1.6% pH 3–10 and 0.4% pH 5–7). The first dimension (isoelectric focusing) was performed on 3 × 125 mm tubes using the Model 225 tube gel casting stand and tube gel adapter (Bio-Rad, Mississauga, Canada) for the Protean II xi cell (Bio-Rad), during which proteins are separated according to their isoelectric points. The second dimension (SDS-PAGE) was performed using 20 × 20 cm gels with the Protean II xi cell. Two identical gels were prepared: one gel was silver stained (Vorum protocol) according to Mortz *et al.* (11) to visualize the separation pattern. The second gel was transferred onto 0.45 µm PVDF membrane. Polymer blot analysis and identification of pADPr binding proteins by MALDI-TOF MS was performed as described (12).

Peptide polymer blot analysis

Peptides corresponding to the predicted pADPr binding domain of selected proteins found by *in silico* analysis were synthesized using Fmoc solid-phase peptide synthesis with an Applied Biosystems 433A peptide synthesizer (Supplementary Table S4). The quality of peptide synthesis was controlled by MALDI-TOF MS analysis and the purity of peptide was evaluated using analytical HPLC. Peptides were dissolved in TBS-T (10 mM Tris-HCl

pH 8.0, 150 mM NaCl, 0.1% Tween-20). One microgram of each peptide was spotted onto a 21 mm × 50 mm nitrocellulose film-slide (Grace Bio-Labs, Bend, OR, USA), air-dried, rinsed three times with TBS-T and incubated for 1 h at room temperature with gentle agitation in TBS-T containing 250 nM ³²P-labeled pADPr synthesized as described (12). It was then washed with TBS-T buffer until no radioactivity could be detected in the washes. The membrane was subsequently air-dried and subjected to autoradiography on an Instant Imager (Perkin Elmer, Woodbridge, Canada), which analyzes and quantifies the distribution of radioactivity on flat samples.

pADPr immunoprecipitation

SK-N-SH cells were seeded onto three 150 mm cell-culture dishes and grown up to 80–90% confluency. Cells were incubated with freshly prepared 100 µM MNNG for 5 min before extraction. All further steps were performed on ice or at 4°C. Two PBS washes were carried out prior to the extraction with 2 ml/plates of lysis buffer [20 mM Tris-HCl pH 7.5, 150 mM NaCl, 0.5% NP-40, CompleteTM protease inhibitor cocktail (Roche Applied Science, Indianapolis, IN, USA)]. Cell lysates were pooled, adjusted to 2 M NaCl and placed on ice for 15–20 min. After 30 s of gentle mixing, the cell extract was extensively dialyzed against ice-cold lysis buffer. Immunoprecipitation experiments were performed using DynabeadsTM magnetic beads covalently coupled with Protein G (Invitrogen, Burlington, Canada). The DynabeadsTM were washed two times with 1 ml of 0.1 M sodium acetate buffer, pH 5.0, coated with 10–15 µg of mouse monoclonal anti-pADPr antibody clone 10H (Tulip Biolabs, West Point, PA, USA) or equivalent amount of normal mouse IgGs (Calbiochem-EMD Biosciences, San Diego, CA, USA). The antibody-coupled DynabeadsTM were incubated for 1 h at room temperature with 1 ml of PBS containing 1% (w/v) BSA (Sigma-Aldrich, Oakville, Canada) to block nonspecific antibody binding sites. The beads were finally washed three times with 1 ml of lysis buffer and added to the pADPr-protein extract for 2 h incubation with gentle agitation. Samples were washed three times with two volumes of lysis buffer for 5 min. Protein complexes were eluted using 150 µl of 3 × Laemmli sample buffer containing 5% β-mercaptoethanol and boiled for 5 min in a water bath. Proteins were resolved using 4–12% CriterionTM XT Bis-Tris gradient gel (Bio-Rad) and stained with Sypro Ruby (Bio-Rad) according to the manufacturer's instructions. Images were acquired using a CCD-based Chemi-Imager 4000 imaging system and AlphaEase software 3.3 (Alpha Innotech Corporation, San Leandro, CA, USA).

PARG activity assays

³²P-labeled automodified PARP-1 was synthesized essentially as described by Ménard and Poirier (13) in a total reaction volume of 900 µl containing 100 mM Tris-HCl, pH 8.0, 10 mM MgCl₂, 8 mM dithiothreitol, 10% (v/v) glycerol, 23 µg of calf thymus-activated DNA (Sigma-Aldrich), 1 mM NAD and 75 µCi of ³²P-labeled NAD (GE Healthcare, Baie d'Urfée, Canada). Ethanol

was added to this preparation dropwise to 10% (v/v) final concentration, with constant mixing, and the reaction mixture was incubated for 3 min at 30°C. The reaction was started by adding 20 U of PARP-1 purified up to the DNA-cellulose step as described by Zahradka and Ebisuzaki (14). After 30 min at 30°C, during which time the enzyme was modified by covalent linkage of pADPr chains to its automodification domain, 100 µl of 3 M sodium acetate, pH 5.2 and 700 µl of propan-2-ol were added as described by Brochu *et al.* (15). The reaction mixture was kept on ice for 30 min and then centrifuged at 10 000g for 10 min at 4°C. The pellet was washed twice with ice-cold 80% (v/v) ethanol, resuspended and incubated at 60°C for 2 h in 1 ml containing 1 M KOH and 50 mM EDTA to release the pADPr from automodified PARP-1 by alkali digestion. Protein-free pADPr was purified on dihydroxyboronyl Bio-Rex (DHBB) affinity resin as described in Shah *et al.* (16). PARP activity was measured by analyzing the production of ADP-ribose monomers from *in vitro* synthesized protein-free pADPr. PARP extracts used for immunoprecipitation experiments were incubated with 10 µM ³²P-labeled pADPr for 20 min at 30°C. Aliquots were then spotted on PEI-F (polyethyleneimine F) cellulose thin layer chromatography (TLC) sheets (Macherey-Nagel, Bethlehem, PA, USA) and developed in 0.3 M LiCl and 0.9 M ethanoic (acetic) acid according to Ménard and Poirier (13).

Immunoblotting

Protein extracts eluted from DynabeadsTM were separated on SDS-PAGE and then transferred onto 0.2 µm nitrocellulose membrane (Bio-Rad). After incubating 1 h with blocking solution (PBS-T containing 5% nonfat milk), the membrane was probed overnight at room temperature with shaking, by primary antibodies to PARP-1 [clone C2-10 (1:5000)], pADPr [10H (1:2500) Tulip Biolabs, 96-10 (1:5000)], IQGAP1 [(1:1000) Cell Signaling], Apoptosis-inducing factor (AIF) [(1:5000) Sigma], Ku80 [(1:5000) Oncogene Research Products, San Diego, CA, USA], DNA-PK [(1:5000) Calbiochem], Adaptins α/β/γ [(1:1000/1:5000/1:5000) BD Biosciences, Mississauga, Canada]. After washing with PBS-T, species-specific horseradish peroxidase-conjugated secondary antibody was added for 1 h at room temperature. Signals were detected with Western LightningTM Chemiluminescence reagent plus kit (Perkin Elmer).

LC-MS/MS analysis

SDS-PAGE protein lanes corresponding to control and anti-pADPr immunoprecipitated extracts were cut into 33 gel slices per lane using a disposable lane picker (The Gel Company, CA, USA). Gel slices were deposited into 96-well plates. In-gel protein digest was performed on a MassPrepTM liquid handling station (Waters, Mississauga, Canada) according to the manufacturer's specifications and using sequencing-grade modified trypsin (Promega, Madison, WI, USA). Peptide extracts were dried out using a SpeedVacTM.

Peptide extracts were separated by online reversed-phase (RP) nanoscale capillary LC (nanoLC) and

analyzed by electrospray MS (ES MS/MS). The experiments were performed on a Thermo Surveyor MS pump connected to a LTQ linear ion trap mass spectrometer (Thermo Electron, San Jose, CA, USA) equipped with a nanoelectrospray ion source (Thermo Electron, San Jose, CA, USA). Peptide separation took place within a PicoFrit column BioBasic C18, 10 cm × 0.075 mm internal diameter (New Objective, Woburn, MA, USA) with a linear gradient from 2% to 50% solvent B (acetonitrile, 0.1% formic acid) in 30 min, at 200 nl/min. Mass spectra were acquired using data-dependent acquisition mode (Xcalibur software, version 2.0). Each full-scan mass spectrum (400–2000 m/z) was followed by collision-induced dissociation of the seven most intense ions. The dynamic exclusion function was enabled (30 s exclusion), and the relative collisional fragmentation energy was set to 35%.

Interpretation of tandem MS spectra

All MS/MS samples were analyzed using Mascot (Matrix Science, London, UK; version 2.2.0). Mascot was set up to search against human Uniref_100 protein database assuming a digestion with trypsin. Fragment and parent ion mass tolerance were, respectively, of 0.5 Da and 2.0 Da. Iodoacetamide derivative of cysteine was specified as a fixed modification. Deamidation of asparagines and glutamine, acetylation of lysine and arginine and oxidation of methionine were specified as variable modifications. Two missed cleavages were allowed.

Criteria for protein identification

Scaffold (version 01_07_00; Proteome Software Inc., Portland, OR, USA) was used to validate MS/MS-based peptide and protein identifications. Peptide identifications were accepted if they could be established at >80.0% probability as specified by the Peptide Prophet algorithm (17). Protein identifications were accepted if they could be established at >90.0% probability and contained at least two identified peptides. Protein probabilities were assigned by the Protein Prophet algorithm (18). Proteins that contained similar peptides and could not be differentiated based on MS/MS analysis alone were grouped to satisfy the principles of parsimony. Using these stringent identification parameters, the rate of false positive identifications is <1%.

Modeling of pADPr-associated protein networks

A graphical representation of the functional connections between pADPr-associated proteins was first computed using filtered Bibliosphere (Genomatix Software, Ann Arbor, MI, USA) interaction maps (co-citation functional level B2). Bibliosphere outputs a bibliometric-based clustering of related genes. Searching for biological processes enrichment of the pADPr binding network against the whole Gene Ontology (GO) hierarchy was performed using BiNGO v2.0 [19] and visualized with Cytoscape v2.5 [20]. GO annotation's *P*-values were obtained by hypergeometric statistical testing (cluster versus the whole-annotation bank) and corrected using the Benjamin and Hochberg false discovery rate included in

the BiNGO software. GO database was downloaded on 1 July 2007. GoMiner [21] was used to reveal protein distributions within selected GO categories. For both *in silico* analysis, gene identification codes were converted or retrieved using the protein's Swiss-Prot accession numbers.

Evaluation of protein domain and family distribution

The Pfam (<http://pfam.sanger.ac.uk/>) domains were obtained by parsing the 'swisspfam' (version Pfam 22.0, July 2007, 9318 families) database using in-house Ruby scripts (version 1.8.6) which output Microsoft Excel-compatible spreadsheets suitable for further analysis. Datasets were generated from the both the original and refined pADPr binding motifs, and the protein dataset that contains all the proteins identified by LC-MS/MS from pADPr immunoprecipitation experiments.

RESULTS

In silico identification of noncovalent pADPr binding proteins

There are currently three protein modules known to bind pADPr. However, they differ greatly in their abundance within the human proteome. The macro domain that has been demonstrated to bind pADPr (4,5) (A1pp) could only be found in 27 human proteins using the InterPRO (22) protein database. Human proteins with the conserved zinc-finger motif PBZ are even rarer, since there are only four human proteins reported to match this stringent motif. On the other hand, 862 human putative pADPr binding proteins were extracted from the Swiss-Prot database following a similarity search based on the noncovalent pADPr binding motif defined by Pleschke *et al.* (3) found within DNA damage checkpoint proteins (Supplementary Table S1). This pADPr binding sequence is based on the consensus motif *hxbxhbbhhb* (where *h* stands for hydrophobic residues, *b* for basic residues and *x* for any amino acid residues). However, the level of conservation of the proposed pADPr binding motif is low but still characterized by preferred amino acid residues and some more variable positions. This is a rather broad pADPr binding signature that can be found in a much larger diversity of proteins than the macro domain and zinc-finger motifs. Consequently, we searched for human proteins with a high similarity level but without any strict requirement for specific amino acids at a given position within the pADPr binding sequence, except for the two positively charged lysine or arginine residues in the center of the motif which seem to be the less tolerant positions. Following these criteria, we screened the Swiss-Prot protein library using the PatsInProt search engine (9) with a similarity level threshold of 90% which allows the detection of degenerated sequences. The resulting dataset of more than 800 proteins (Supplementary Table S1) represents an impressive number of proteins. Although it probably displays a high rate of false positives, this *in silico* screening test is considered valuable because it greatly increase the likelihood of detecting a pADPr binding protein.

Refinement of the original pADPr binding motif

We first wanted to increase the number of experimentally validated pADPr binding sites so as to better define a consensus pADPr binding pattern and get a more representative view of the amino acid frequency at any given position. To achieve this goal, we selected some putative pADPr binding proteins suspected to be involved in pADPr-associated biological processes and synthesized peptides that corresponded to the region most similar to the consensus pattern. Table 1 presents the comprehensive list of pADPr binding regions that have been tested using synthetic peptides in polymer blot assays. For the present study, 24 new peptides were synthesized and assayed for pADPr binding. The hnRNP A1 peptide was used as a positive control since it has been validated as a strong and specific pADPr binding peptide (12). About one-third of the new peptides (9 out of 24) were characterized as pADPr binding peptides (Figure 2A). Most of the validated pADPr binding peptides share a restricted set of amino acids at specified positions of the pADPr binding consensus sequence (Figure 2B) from which we can derive a refined consensus motif. This modified consensus sequence with a much more limited set of amino acids at conserved positions, [HKR]₁-X₂-X₃-[AIQVY]₄-[KR]₅-[KR]₆-[AILV]₇-[FILPV]₈, represents a more stringent version of the original consensus sequence proposed by Pleschke and collaborators (3). In contrast to the more relaxed consensus, the two positively charged amino acids residues [KR]₅-[KR]₆ are strictly followed by either A, I, L or V ([AILV]₇) which are classified as residues with alkyl side chains. These strong pADPr binding regions do not require a conserved hydrophobic residue at position 3, but the positively charged amino acid residues at position 1 is conserved. This refined pattern of validated pADPr binding sites is conserved in histone H4 (23,24) and hnRNP A1, whose pADPr binding motifs have been validated experimentally as strong binding sites (12).

The refined pattern was searched without mismatch tolerance against the Swiss-Prot database to extract a sub-dataset of pADPr binding proteins with high similarity to the pADPr binding sites that were validated in our study (Supplementary Table S2). Interestingly, the 526 unique proteins in this dataset are much better connected to DNA and chromatin functions than the original dataset. Unique proteins to the dataset generated with the refined pADPr binding motif include: DNA excision repair proteins ERCC-2 and ERCC-6, DNA polymerase subunit alpha B, DNA primase small subunit, DNA replication licensing factors MCM3, MCM5, MCM7, DNA topoisomerase 2-beta, mitochondrial DNA topoisomerase I, SWI/SNF-related matrix-associated actin-dependent regulator of chromatin subfamily A member 5 (SMCA5), Centromere protein T (CENP-T), the DNA damage checkpoint response protein HUS 1, several histone metabolism-associated proteins, such as the histone acetyltransferases MYST3, MYST4, histone acetyltransferases p300 (25) and PCAF (26), or the newly identified pADPr binding protein DEK (27). Because several of these proteins are closely related to known pADPr-modulated pathways, the refined consensus appears to

Table 1. Comprehensive protein sequence alignment of predicted pADPr binding motifs screened by polymer blot analysis

Swiss-Prot accession	Protein description	Sites	pADPr binding motif	Binding	Reference
Synthetic peptides assayed in this study (see Figure 2A)					
Q9NWT8	Aurora-A kinase interacting protein	132–153	KIRRRKMNHKKYRKLVKKTRFL	+	This study
Q96GD4	Serine/threonine-protein kinase Aurora-B	182–203	EELADALMYCHCKKVIHRDIKP	–	This study
P55957	BH3-interacting domain death agonist [BID]	145–166	EKTKMLVLALLLAKKVASHTPSL	+	This study
P38398	Breast cancer type 1 susceptibility protein [BRCA]	123–144	SI IQSMGYRNRKRLIQSEPEN	–	This study
Q9BXL7	Caspase recruitment domain protein 11 [CAR-11]	740–761	VTLHYKVNHEGYRKLVKDMEDG	–	This study
P49450	Centromere protein A [CENP-A]	51–72	IRKLRKSTHLLTRKLPFSRLAR	+	This study
Q12798	Centrin-1	58–79	RALGFEPKKEEMKKMISEVDRE	–	This study
Q13616	Cullin-1	460–481	DVFKQFYAKMLAKRLVHQNSAS	–	This study
Q03468	DNA excision repair protein ERCC-6	284–297	ERKKGCCNKRAARKAPAPVTPP	+	This study
Q5VTC7	Hexokinase domain-containing protein 1	420–441	HPQYPKRLHKVVRKLVPSCDVR	+	This study
A4QPB0	IQ motif containing GTPase activating protein 1 [IQGAP1]	1413–1435	SEQEAEHQRAMQRRAIRDAKTP	–	This study
Q76GR4	DNA ligase 1	46–67	VSESDSPVKRPGKKAARVLGSE	–	This study
P43246	DNA mismatch repair protein MSH2	806–827	TTEETLTMLYQVKKGVCDQSFQ	–	This study
P19367	Hexokinase-1	420–441	HPQYSRRFHKTLRRLVPSDVR	–	This study
Q14764	Major vault protein MVP	499–520	SLSAGRPKRPHARRALCLLLGQ	+	This study
Q15172	Serine/threonine-protein phosphatase 2A 56 kDa regulatory subunit alpha isoform	18–39	SEKVDGFTKSKVRKAQRQKRSQ	–	This study
O60264	SWI/SNF-related matrix-associated actin-dependent regul. of chromatin A5 [SMCA5]	906–927	RGEARIQRRISIKKALDTKIGR	–	This study
P11387	DNA topoisomerase 1	263–284	MLDHEYTTKELEFRKNFKDWRK	–	This study
P11387	DNA topoisomerase 1	533–554	DSIRYYNKVPEKRVFKNLQLF	–	This study
P11387	DNA topoisomerase 1	669–690	KADAKVMKDAKIKKVVESKKA	–	This study
Q02880	DNA topoisomerase 2-beta	736–757	IPSLVDGFKPGQRKVLFTCFKR	+	This study
O43684	Mitotic checkpoint protein BUB3	145–166	VSGDRLIVGTACRRRLVWDLRN	+	This study
P24941	Cell division protein kinase 2 [CDK2]	76–97	LYLVFEFLHQDLKKFMDASALT	–	This study
Q15021	Condensin complex subunit 1	518–539	GRIYQLLAKASVKKKAIILTREA	+	This study
P09651	Heterogeneous nuclear ribonucleoprotein A1 [hnRNP A1]	93–114	EDSQRPGAHLTVKKKIFVGGIKE	+	This study + (12)
Peptides assayed in other studies					
P22626	Heterogeneous nuclear ribonucleoprotein A2/B1	100–121	EESGKPGAHVTVKKLIFVGGIKE	+	(12)
P10155	60 kDa SS-A/Ro ribonucleoprotein	138–158	SMKCGMWR-ALRKAADWYNE	+	(12)
P62805	Histone H4	24–45	RDNIQGITKPAIRRLARRGGVK	+	(12)
P49959	Double-strand break repair protein MRE11	564–585	AATNKGRGRGRGRGGRGQNSA	+	(45)
Q13315	Serine-protein kinase ATM	98–119	SSLVKYFIKCANRRAPRLKQCE	+	(46)
Q13315	Serine-protein kinase ATM	2734–2755	MCNTLLQRNTETRKRKLITICTY	+	(46)
P29966	Myristoylated alanine-rich C-kinase substrate [MARCKS]	149–170	ETPKKKKRFSEFKKSEKLSGFS	+	(3)
P52701	DNA mismatch repair protein MSH6	299–319	KRKRMTVNGNSLKRKKSSRKET	+	(3)
P38936	Cyclin-dependent kinase inhibitor 1 [p21]	143–164	QTSMTDFYH-SKRRLTFSKRKP	+	(3)
P23025	DNA repair protein complementing XP-A cells [XPA]	205–226	EVRQENREKMKQKKFDKVKKEL	+	(3)
P18887	DNA repair protein XRCC1	382–403	RKEWVLDCHRMRRRLPSRRYLM	+	(3)
P49916	DNA ligase III	18–39	KKCKEKIVK-GVCRIGKVVVNP	+	(3)
Q07864	DNA polymerase epsilon catalytic subunit A	720–741	KRLADYCRKAYKKIHIITKVEE	+	(3)
P12956	DNA repair protein XRCC6 [Ku70]	232–253	HFEESKLEDLIRKVRAKETRK	+	(3)
P78527	DNA-dependent protein kinase catalytic subunit [DNA-PK]	2733–2754	MRDQEKLSLMYARKGVAEQKRE	+	(3)
Q00653	Nuclear factor NF-kappa-B p100 subunit	170–191	QRELEQEAKELEKKVMDLSIVR	+	(3)
P35228	Nitric oxide synthase, inducible [NOS2]	498–519	THVWQDEKRRPKRREIPLKVLV	+	(3)
O76075	DNA fragmentation factor subunit beta [CAD]	144–165	GLFSRFQSKSGYLRYSCESRIR	+	(3)
O14746	Telomerase reverse transcriptase	960–981	FNRGFKAGRNMRKRLFGVLRLLK	+	(3)
P43246	DNA mismatch repair protein MSH2	230–251	ADFSTKDIYQDLNRLKGGKGE	–	(3)
P38936	Cyclin-dependent kinase inhibitor 1 [p21]	8–28	VRQNPCGSK-ACRRLFGPVDSE	–	(3)
P23025	DNA repair protein complementing XP-A cells [XPA]	22–42	ASVRASIER-KRQRALMLRQAR	–	(3)
P13010	DNA repair protein XRCC5 [Ku86]	17–138	VIQHETIGKKFKRHEIIFTDL	–	(3)
P49916	DNA ligase III	779–800	SRKAPSKPSASTKKAEGKLSNS	–	(3)
Q6DRD3	DNA polymerase beta	22–42	ANYERNVNR-ATHKYNAYRKAA	–	(3)
Q6DRD3	DNA polymerase beta	34–55	KYNAYRKAASVIAKYPQKIKSG	–	(3)

The alignment includes known and putative pADPr binding proteins based on the pADPr binding motif (hxbxhbbhbh)(3). The central amino acid couple K/R is shown on a black background. Proximal residues that fit the consensus are indicated under a gray background. Swiss-Prot accession codes, sites mapping and experimental pADPr binding validation are indicated for each peptide.

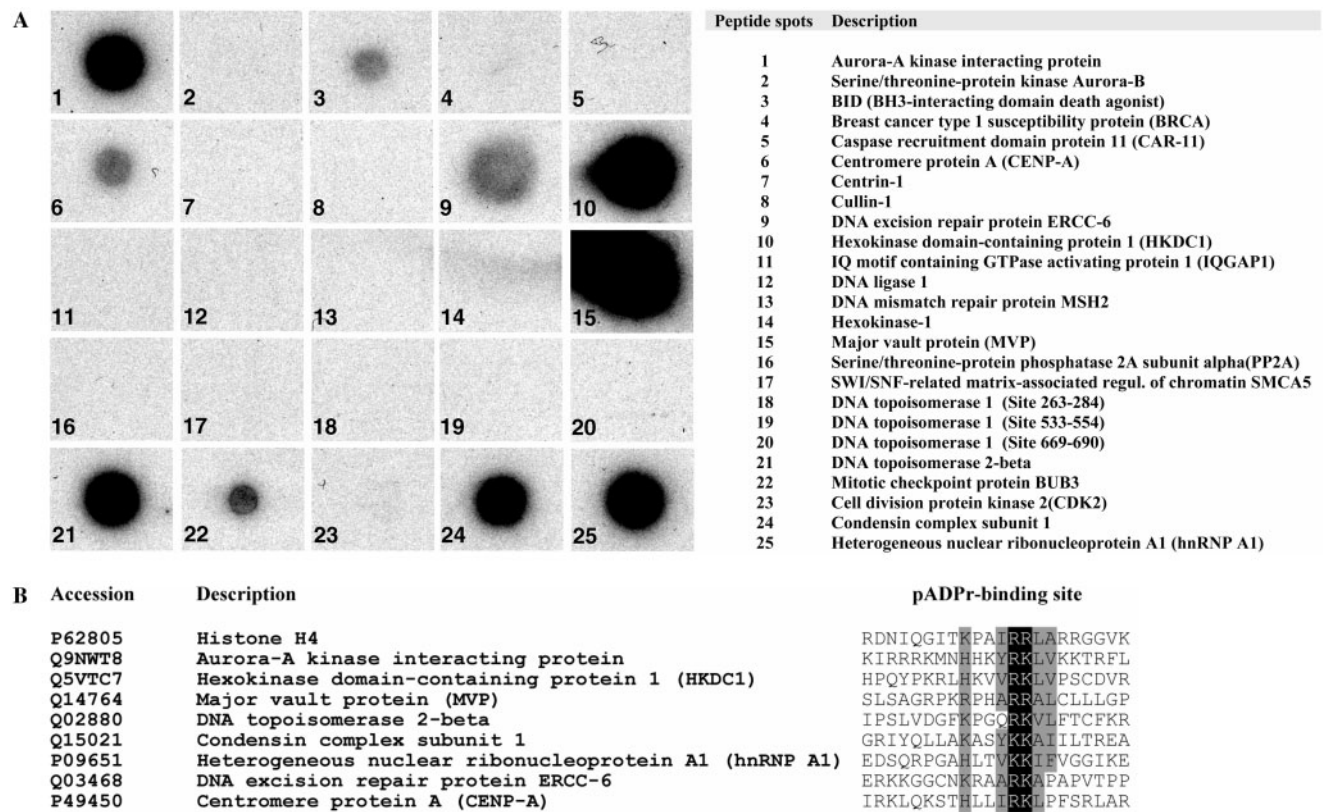


Figure 2. Polymer blot analysis. (A) Synthetic peptides corresponding to putative pADPr binding proteins as revealed by *in silico* prediction based on the consensus sequence proposed by Pleschke *et al.* (3) were dot-blotted onto nitrocellulose-coated glass slides, screened with ³²P-pADPr and autoradiographed (see Supplementary Table S1 for the complete list of predictions). Amino acid sequences used for peptide synthesis are provided in Supplementary Table S4. (B) A refined pADPr binding consensus is generated from the sequence alignment of validated pADPr binding peptides. Experimentally verified pADPr binding regions from pADPr dot blot analysis were aligned to derive a refined pADPr binding motif and to computationally screen protein sequence database with the goal of achieving higher reliability and minimizing false positive identifications (see Supplementary Table S2 for a listing of proteins that match the refined pADPr binding consensus).

have a much higher specificity than its more relaxed counterpart. This refined motif lowers the screening effort to a more manageable level and should be considered as a first step in an attempt to identify pADPr binding proteins.

Identification of noncovalent pADPr binding proteins by polymer blot analysis following two-dimensional electrophoresis

As *in silico* predictions are still limited in their ability to identify all pADPr binding proteins, it mostly serves a rapid approach to identify putative pADPr binding targets. Until they are more accurate, *in silico*-identified pADPr binding proteins will need to be validated experimentally. Thanks to the development of high-throughput proteomics technologies, proteome-wide identification of pADPr binding proteins is now manageable. Half a milligram of HeLa cell protein extract was resolved into discrete spots by two-dimensional electrophoresis and transferred onto PVDF membrane. pADPr binding

proteins were identified by matrix-assisted laser desorption ionization (MALDI) MS after incubation with ³²P-labeled pADPr and autoradiography (Figure 3). We selected tube-gel two-dimensional electrophoresis instead of the more recent immobilized pH gradient (IPG) two-dimensional isoelectric focusing (IEF) because of the increased sample loading capacity and because reproducibility was not as important as it would have been in a differential proteome analysis. Most of the pADPr binding proteins are found at high pH values (positively charged) as we would expect for proteins involved in DNA/RNA transactions or specifically involved in the binding of a negatively charged polyanion, such as pADPr. Known pADPr binding proteins, such as hnRNPs (12) still represent many of the abundant pADPr binding proteins identified by this method (Table 2). DNA-binding proteins, such as members of the zinc-finger protein family, are also found in several spots. In addition, the presence of the major vault protein (MVP) is interesting since its pADPr binding region,

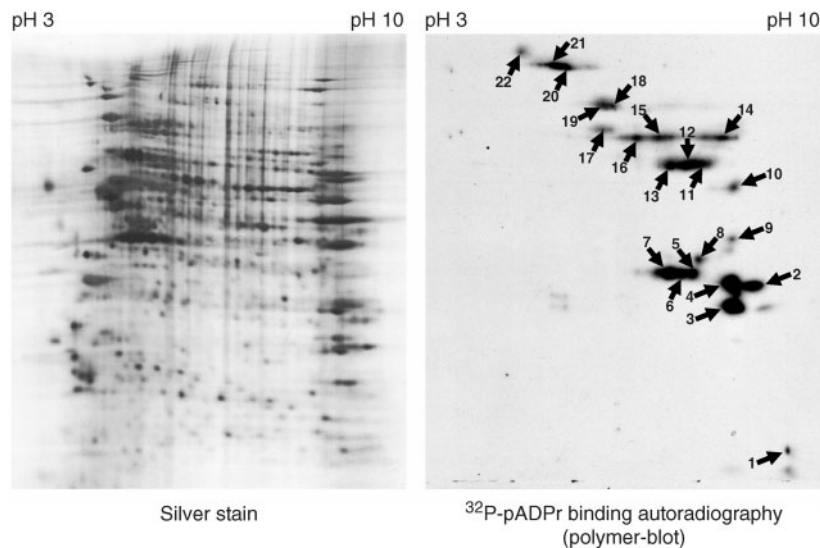


Figure 3. Two-dimensional polymer blot analysis. HeLa cell extracts were separated by tube-gel isoelectric focusing, resolved by SDS-PAGE and transferred onto PVDF membrane. The left panel shows the bidimensional protein separation as revealed by silver staining. The right-hand panel shows a corresponding two-dimensional-gel transferred onto a PVDF membrane for polymer blot analysis. Incubation with ^{32}P -pADPr followed by autoradiography reveals a binding-protein pattern. Numbered spots were excised for identification by peptide mass fingerprinting (see Table 2 for complete spot identifications).

targeted in the peptide-binding assay, is the strongest of all tested (Figure 2A). Other proteins identified by MALDI MS also contain a pADPr binding site that match the refined consensus motif, including DNA replication licensing factor MCM5, Cullin 1 and Cullin 4A. Cell-cycle regulators CDK1 and CDK2 are also noteworthy identifications as well as Caspase-10. The identification of electrophoretically transferred, two-dimensionally separated proteins by MS suffers important limitations since high molecular weight proteins are particularly difficult to analyze this way and multiple co-migrating proteins in single spot can lead to ambiguous identifications.

Immunoprecipitation of pADPr-associated proteins following alkylation-induced DNA damage

The large-scale validation and identification of pADPr binding proteins mostly relied on polymer blot analysis projects based on one- or two-dimensional electrophoresis, both techniques requiring heavy denaturation steps for protein separation. An alternative approach to explore the nature of the interaction between cellular proteins and pADPr under more physiological conditions and with increased dynamic range is to use specific anti-pADPr antibodies to immunoprecipitate pADPr-associated proteins and pADPr-containing protein complexes. However, even if pADPr synthesis can be achieved by several PARPs, basal levels of pADPr in unstimulated cells are extremely low and probably insufficient to allow the identification of pADPr binding proteins in the absence of PARP-1 activation. Therefore, we used genotoxic stress to trigger activation of PARPs and thereby increase pADPr levels by 10- to 500-fold (2), up to concentrations appropriate for affinity purification. Nonetheless, because of the transient nature of pADPr following PARPs activation in response to DNA strand breaks, we needed a

model in which pADPr levels would be sustained. Moreover, we needed a protein extraction procedure that would extract nuclear matrix-associated proteins since this structure represents a major site of pADPr metabolism. Indeed, Cardenas-Corona and colleagues (28) have shown that most of the pADPr is associated with the nuclear matrix and possibly tightly embedded within it since DNase treatments are inefficient to release pADPr. In order to circumvent these two difficulties, pADPr hydrolysis was first significantly reduced by knocking down endogenous PARG in SK-N-SH cells, one of the most extensively studied neuroblastoma cell line used as a model for cytotoxicity, radiobiology and DNA damage response. With respect to the second concern, we performed high salt protein extractions, a procedure that has shown optimal results for the release of chromatin-bound pADPr. Extracts dialyzed against a non-denaturing immunoprecipitation buffer were used to pull-down pADPr and pADPr-associated proteins.

Figure 4A and B show that impaired pADPr turnover in PARG siRNA-treated cells results in sustained levels of pADPr. In contrast, pADPr levels in untreated cells do not increase as much and start decreasing after 10 min. Long-term PARG siRNA treatment (6 days) was necessary to reduce endogenous PARG levels by 80% as estimated from TLC PARG activity assays (Figure 4C and D), a maximum in PARG expression knockdown also reported by Cohausz *et al.* (29) in a pADPr-metabolizing enzymes study on alkylation-induced cell death. We coupled anti-pADPr mouse monoclonal antibodies (clone 10H) to magnetic Protein-G coated Dynabeads[®] to selectively pull-down pADPr-associated proteins. Normal mouse IgGs were used as a control reagent for immunoprecipitations using mouse monoclonal antibodies. Immunoprecipitated proteins were stained using SYPRO Ruby fluorescent stain after 1D SDS-PAGE

Table 2. Identification of pADPr binding proteins by MALDI-TOF MS

Spot number	Swiss-Prot accession	Protein description	Protein function
1	P10155	60 kDa SS-A/Ro ribonucleoprotein	RNA transcription
	Q9Y6M9	NADH dehydrogenase 1 beta subcomplex subunit 9	Mitochondrial electron transport
	O76080	AN1-type zinc-finger protein 5	May be involved in transcriptional regulation
2	P09651	Heterogeneous nuclear ribonucleoprotein A1 (hnRNP A1)	RNA transcription
	P17098	Zinc-finger protein 8	May be involved in transcriptional regulation
3	P56202	Cathepsin W	Cysteine-type peptidase activity
	P23193	Transcription elongation factor A protein 1	RNA transcription
	P06493	Cell-division control protein 2 homolog (CDK1)	Cell-cycle progression and RNA transcription
	P24941	Cell-division protein kinase 2 (CDK2)	Cell-cycle progression and RNA transcription
4	P09651	Heterogeneous nuclear ribonucleoprotein A1 (hnRNP A1)	RNA transcription
	P17038	Zinc-finger protein 43	May be involved in transcriptional regulation
5	P22626	Heterogeneous nuclear ribonucleoproteins A2/B1	RNA transcription
6	P51523	Zinc-finger protein 84	May be involved in transcriptional regulation
	P17024	Zinc-finger protein 20	May be involved in transcriptional regulation
7	P50458	LIM/homeobox protein Lhx2	RNA transcription
	O00257	E3 SUMO-protein ligase CBX4 (Polycomb 2 homolog)	RNA transcription
	P22626	Heterogeneous nuclear ribonucleoproteins A2/B1	RNA transcription
	P22626	Heterogeneous nuclear ribonucleoproteins A2/B1	RNA transcription
8	Q9UK10	Zinc-finger protein 225	May be involved in transcriptional regulation
	P33992	DNA replication licensing factor MCM5	DNA replication
	O14628	Zinc-finger protein 195	May be involved in transcriptional regulation
	P51523	Zinc-finger protein 84	May be involved in transcriptional regulation
9	No identification		
10	P04720	Elongation factor 1-alpha 1	Translational elongation
11	P06213	Insulin receptor	Insulin receptor signaling pathway
	P20592	Interferon-induced GTP-binding protein Mx2	GTPase activity
	P11171	Protein 4.1	structural constituent of cytoskeleton
	Q02928	Cytochrome P450 4A11	Fatty acid metabolic process
	P31948	Stress-induced-phosphoprotein 1	Response to stress
	P50458	LIM/homeobox protein Lhx2	RNA transcription
	P31948	Stress-induced-phosphoprotein 1	Response to stress
12	Q01742	Fibroblast growth factor receptor 2	Fibroblast growth factor receptor activity
	Q92851	Caspase-10 [Precursor]	Induction of apoptosis
	P09651	Heterogeneous nuclear ribonucleoprotein A1 (hnRNP A1)	RNA transcription
	Q9NZL3	Zinc-finger protein 224	May be involved in transcriptional regulation
13	No identification		
14	No identification		
15	P18206	Vinculin	Cell adhesion
	P26232	Catenin alpha-2	Cell adhesion
	Q13616	Cullin-1	G1/S transition of mitotic cell cycle
	Q14764	Major vault protein	Vaults structure
	O14983	Sarcoplasmic/endoplasmic reticulum calcium ATPase 1	Calcium ion transport
	No identification		
16	No identification		
17	No identification		
18	No identification		
19	No identification		
20	No identification		
21	No identification		
22	No identification		

HeLa cell extracts were separated by two-dimensional gel electrophoresis and the spots corresponding to pADPr binding proteins were revealed by polymer blot analysis. See Figure 3 for spot references.

(Figure 5). 10H-immunoprecipitated proteins are distributed across a wide range of molecular weights with minimal nonspecific binding from the control IgGs.

LC-MS/MS identification of pADPr-associated proteins from SK-N-SH immunoprecipitates

Immunoprecipitated proteins resolved by SDS-PAGE were manually excised from the gel and identified using LC-MS/MS. More than 300 specific proteins were identified with stringent protein identification probabilities criteria as described in Materials and methods section (Supplementary Table S3). Hallmark proteins of the DNA damage response and repair pathways are

collectively over-represented in the pADPr-associated protein dataset (Figure 5), with the notable identification of PARP-1, DNA-PK, XRCC5 (Ku80/86), MSH2, MSH6 and the DNA damage-binding protein 1 (DDB1/Xeroderma pigmentosum group E-complementing protein). There are also several important proteins involved in DNA replication and transcription including DNA replication licensing factors MCM3/MCM4/MCM5/MCM7, and DNA topoisomerase II beta whose corresponding pADPr binding region showed strong interaction with pADPr in polymer blot assays (Figure 2A). The minichromosome maintenance (MCM) proteins are DNA helicases involved in the maintenance of genomic stability in pathways that encompass DNA replication

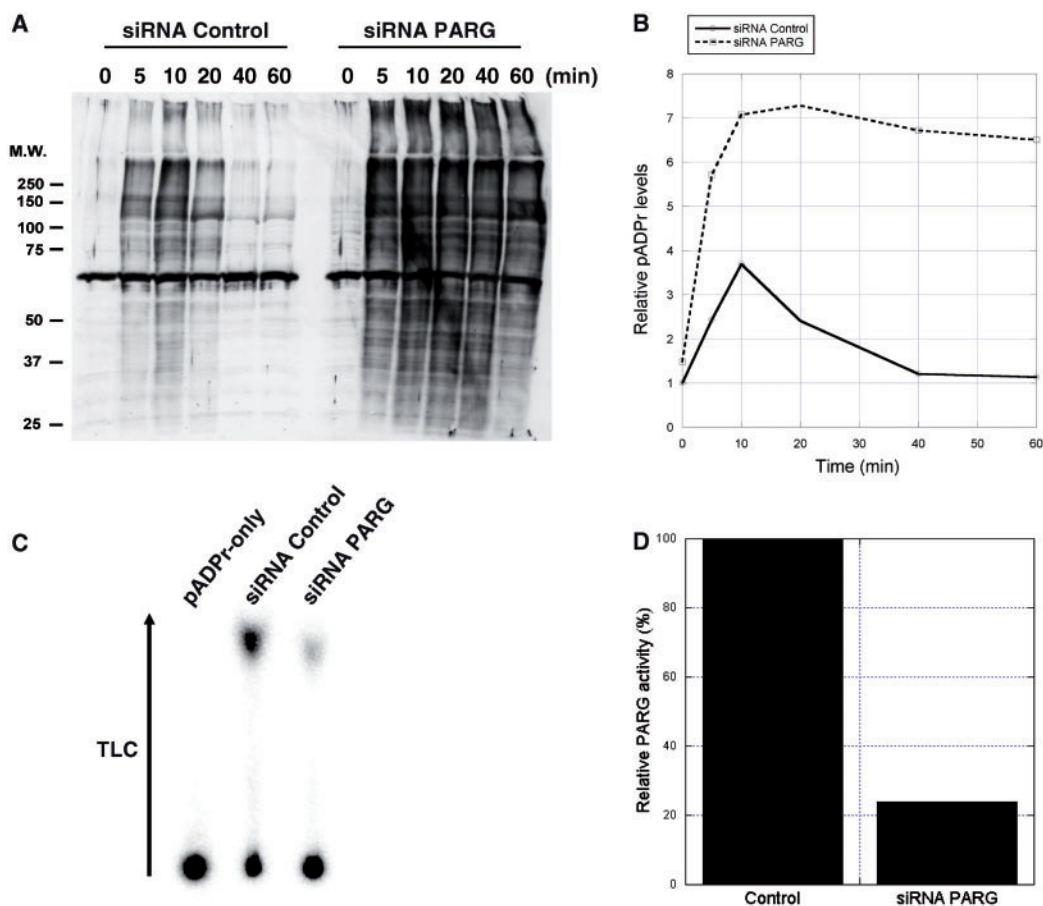


Figure 4. pADPr levels are increased and sustained in SK-N-SH cells treated with PARG siRNA following alkylation-induced DNA damage. (A) Time course western blot analysis of pADPr accumulation in SK-N-SH cells following 100 μM MNNG treatment in both control and PARG siRNA treated cells. Crude protein extracts were loaded and subjected to SDS-PAGE and immunoblotting. Blots were revealed with anti-pADPr polyclonal antibody 96-10 as described in Materials and methods section. (B) Western blot quantification of pADPr levels from control (full line) and PARG siRNA-treated cells (dashed line) following 100 μM MNNG treatment. (C) Evaluation of PARG knockdown using PARG TLC activity assays. Silencing was conducted over 6 days, passaging cells every 48 h to achieve maximum PARG knockdown. Whole-cell extracts were prepared from cultured cells that had been treated with either control or PARG siRNA. PARG activities were detected by TLC analysis of reaction mixtures containing these cell extracts and 32 P-labeled pADPr as a substrate. Substrate remained at the origin of the TLC plate, while ADP-ribose products migrated towards the top of the TLC plate following development by 0.3 M LiCl and 0.9 M ethanoic (acetic) acid. (D) Relative PARG residual activity in SK-N-SH cells after 6-day silencing as determined from the TLC quantification of PARG reaction products.

and repair by catalyzing the transient opening of DNA duplexes (30). Other helicases, such as the RNA helicases (DDX, DHX, DEAD/H families) are also remarkably abundant in the pADPr-associated protein dataset.

The number of observed peptides by LC-MS/MS for a given protein is semi-quantitative as it often reflects the relative abundance of the protein in the analyzed sample. Predominant proteins were estimated from their number of unique peptides. Supplementary Table S3, which lists all the proteins identified by LC-MS/MS in immunoprecipitates, presents the proteins in order of decreasing number of peptides. Proteins identified with high sequence coverage like PARP-1, IQGAP1, DNA-PK or Ku80 (XRCC5) were validated by western blot (Figure 6). In addition, Figure 6 shows that pADPr is selectively enriched in the pull-down extracts. AIF, which had been identified with only two unique peptides, also appeared with high specificity in western blot, thus validating

the MS data. The presence of vesicle-associated adaptins isoforms α , β and γ in pADPr immunoprecipitates was also validated by western blot analysis (Figure 6). Unexpectedly, many vesicular proteins involved in the control of endosomal dynamics, such as the coatamer subunit alpha (COPA) and clathrin-associated adaptor protein AP-2, are also part of the pADPr-associated dataset. It is however noteworthy that adaptor proteins AP-1 and AP-2 as well as golgi-associated proteins are predicted to be pADPr binding proteins based on *in silico* analysis (Supplementary Table S2). These results provide additional support for a link between poly(ADP-ribosylation) and trafficking of endosomal vesicles (31–33).

In silico predictions and experimental discoveries are obviously complementary approaches for the exploration of the pADPr interactome. The LC-MS/MS identification of the splicing factor ASF/SF2 (Supplementary Table S3), a recently reported pADPr binding protein (34), in the

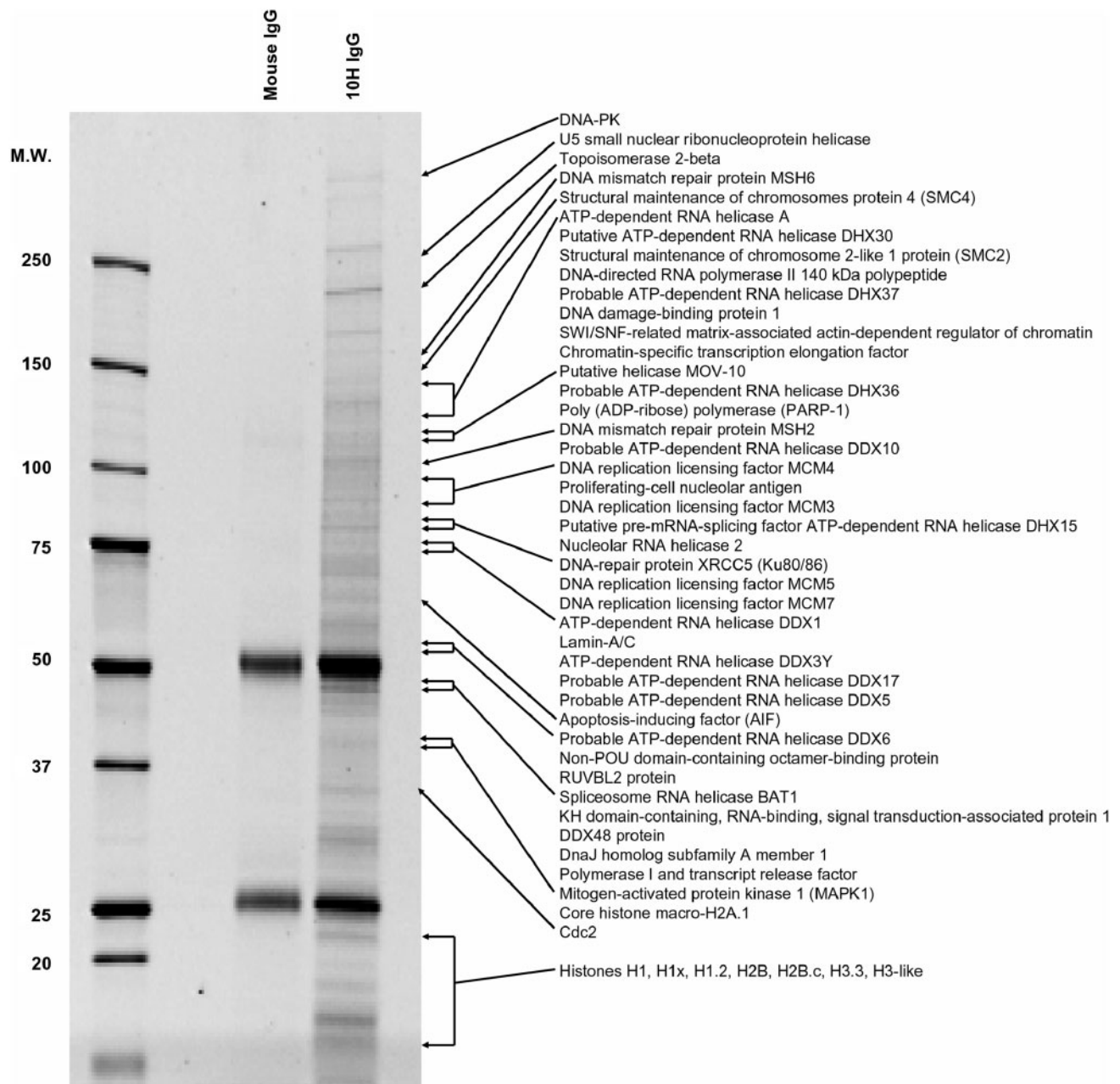


Figure 5. SDS-PAGE analysis of pADPr-associated proteins from MNNG-treated and PARG-silenced SK-N-SH cells after immunoprecipitation with anti-pADPr antibodies. pADPr-associated proteins were immunoprecipitated using anti-pADPr mouse monoclonal antibody clone 10H bound to Protein G coated magnetic beads. Immunoprecipitates were resolved by 4–12% SDS-PAGE and stained with SYPRO Ruby fluorescent dye. Normal mouse IgGs were used to assess nonspecific binding. Selected proteins identified by LC-MS/MS, mostly involved in DNA/RNA transactions, are shown (see Supplementary Table S3 for complete protein listing).

protein dataset generated from pADPr immunoprecipitates illustrate this complementarity since no consensus motifs were able to predict its pADPr binding.

Modeling of pADPr-associated protein networks

Unorganized datasets containing numerous proteins remain hard to analyze and the possibility to draw conclusions is hampered by the apparent complexity. We used systems biology data mining tools to elucidate the dynamic interplay of more than 300 putative pADPr-

associated proteins in our dataset. Based on structured GOs annotations, we first determined which biological process categories were statistically over-represented in the immunoprecipitated pADPr-associated protein dataset. The statistical analysis was performed with a BiNGO (19) implementation in Cytoscape (20). BiNGO is a tool developed to highlight predominant functional themes in a dataset and to visualize them as an integrated molecular interaction network. Figure 7 shows the network distribution of predominant GO terms associated with pADPr-associated proteins in immunoprecipitates.

Proteins involved in DNA/RNA transactions are clearly emerging from the protein population as we would expect. Statistically significant over-represented ontologies of pADPr-associated proteins are grouped into six categories that encompass the major PARP-1-dependent pathways (*chromosome organization and biogenesis*, *DNA repair*, *DNA replication*), pADPr-regulated functions (*progression through cell cycle*) and *mRNA metabolism/protein synthesis* for which several studies suggest a link with poly(ADP-ribosyl)ation reactions (12,35–38).

A literature mining tool called Bibliosphere (Genomatix Software Inc.) was also used to visualize the relations between proteins based on the degree of interconnection

for their corresponding genes (Supplementary Figure S1). In the Bibliosphere generated network, related genes are clustered around ‘hubs’ that play central role in the biological pathways. In this representation, PARP-1 is displayed as the central molecule linking all the pathways. The functional categories revealed by the Bibliosphere network are similar to the results obtained with the GO classification tool. Biological processes, such as structural organization and function of the nucleus and chromatin, cellular response to DNA double-strand breaks, DNA mismatch repair, DNA replication and genome integrity, apoptosis and mRNA metabolism/protein synthesis are predominant and strongly support the

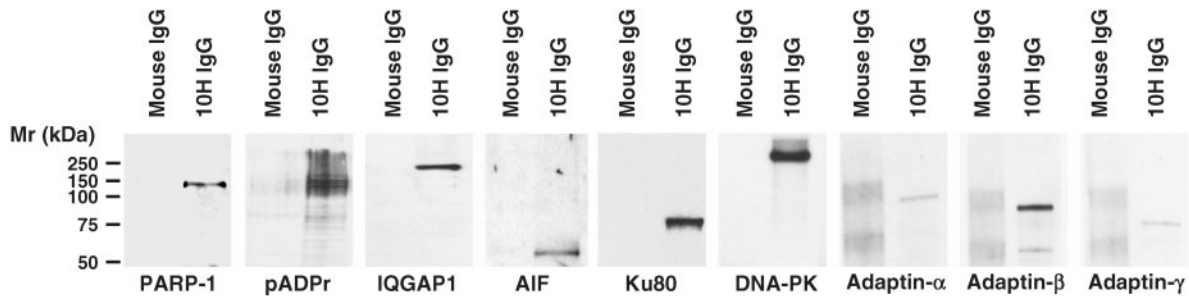


Figure 6. Validation of selected pADPr-associated proteins identified by LC-MS/MS using western blot analysis of pADPr immunoprecipitates. The specificity of the pADPr immunoprecipitation using anti-pADPr 10H monoclonal antibodies was evaluated by immunoblot analysis as described in Materials and methods section. The same proteins were not precipitated by normal mouse IgGs, confirming the specificity of the pull-down.

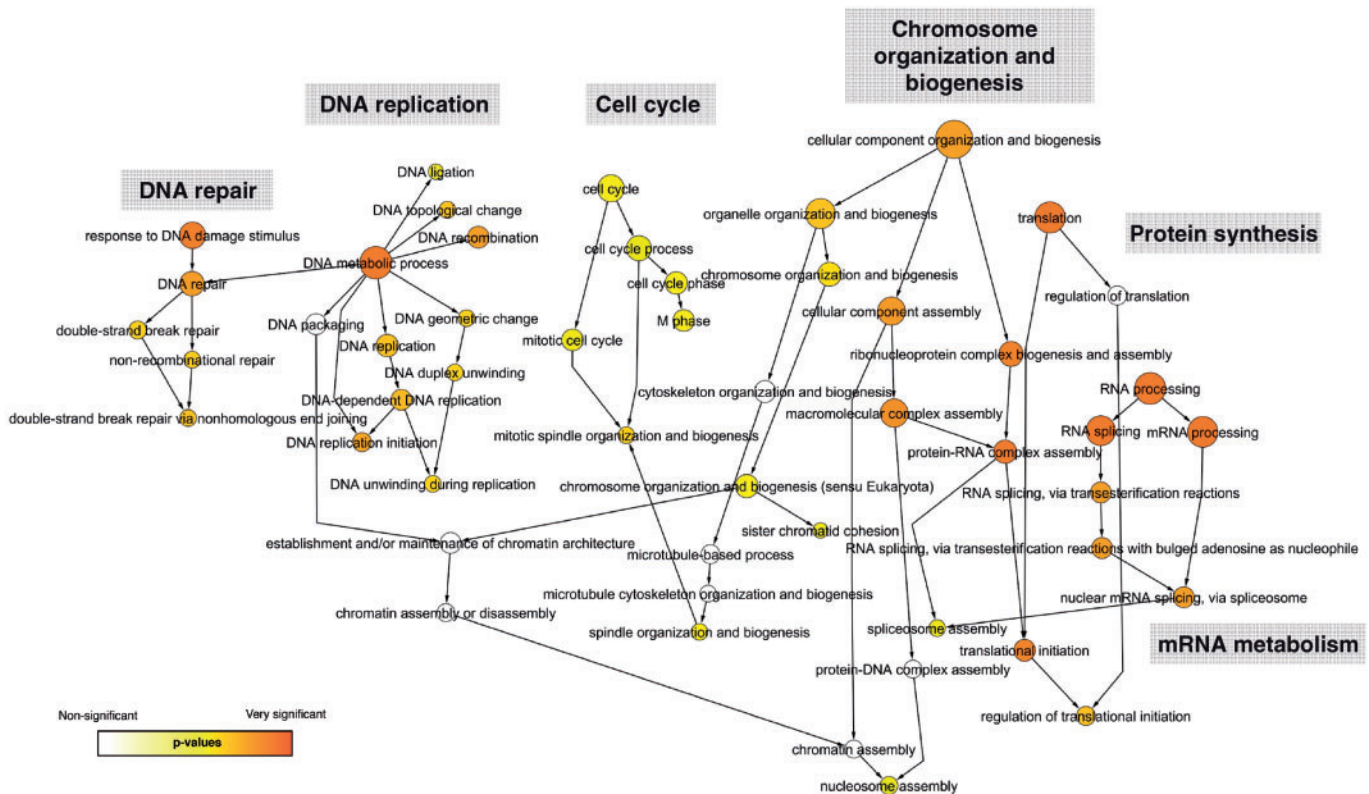


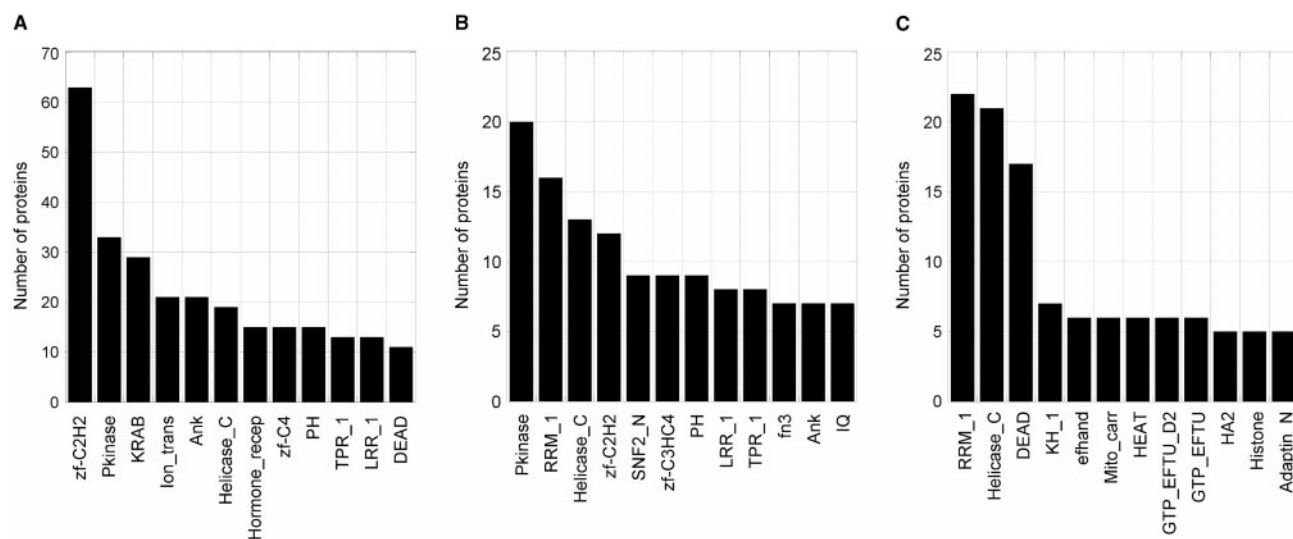
Figure 7. Graphical network representation of pADPr-associated proteins identified by LC-MS/MS in anti-pADPr immunoprecipitates. Functional categorization of pADPr-associated proteins was performed using GO annotations. Over-represented categories were statistically identified using BiNGO and visualized with Cytoscape. The size of the terms (circles) is representative of the proportional protein abundance in the dataset and the color shading indicates the degree of statistical significance (darker shades indicate stronger significance).

classification obtained with BiNGO's molecular interaction graph (Figure 7). BiNGO and Bibliosphere are two independent tools for data integration and visualization that provided converging results. However, they can complement each other and deliver a more global view of the pADPr-associated biological network.

Comparative distribution of pADPr binding candidates in predicted and experimental datasets

An estimation of the predominant protein domains found within the computationally predicted and

experimentally verified pADPr binding protein datasets based on the Pfam protein families database (39) was performed (Figure 8). Clearly, proteins containing the classical zinc-finger motif (zf-C₂H₂) are over-represented in the *in silico* protein dataset obtained through searching a pattern with high similarity to the original motif (Figure 8A). However, the proteins revealed by our refined motif are enriched in additional pathways involving nucleic acids binding (Figure 8B). While zinc-finger proteins still represent an important category, RNA recognition motifs (RRM_1) now occur frequently as they do for the



Pfam Domains	Description	Functions
zf-C2H2	Zinc finger C2H2 type	Nucleic acid-binding
Pkinase	Protein kinase domain	Serine/threonine and tyrosine protein kinases
KRAB	KRAB box	Protein-protein interactions (present in about a third of zinc finger C2H2 proteins)
Ion_trans	Ion transport protein	Sodium, Potassium, Calcium ion channels
Ank	Ankyrin repeat	Protein-protein interactions
Helicase_C	Helicase conserved C-terminal domain	Integral part of the DEA(D/H)-box RNA helicase family / RNA metabolism
Hormone_recep	Ligand-binding domain of nucl. hormone receptor	Molecular switch to turn on transcriptional activity
zf-C4	Zinc finger, C4 type (two domains)	DNA binding domain of nuclear hormone receptor
PH	Pleckstrin homology	Intracellular signaling / constituents of the cytoskeleton
TPR_1	Tetratricopeptide repeat	Mediates protein-protein interactions and the assembly of multiprotein complexes
LRR_1	Leucine Rich Repeat	Structural framework for the formation of protein-protein interactions
DEAD	DEAD/DEAH box helicase	RNA metabolism
RRM_1	RNA recognition motif	RNA-binding
SNF2_N	SNF2 family N-terminal domain	ATPase component of the SNF2/SWI multisubunit complex
zf-C3HC4	Zinc finger, C3HC4 type (RING finger)	Protein-protein interactions
fn3	Fibronectin type III domain	Maintenance of the cellular cytoskeleton
Ank	Ankyrin repeat	Protein-protein interactions
IQ	IQ calmodulin-binding motif	Calcium-binding
KH_1	K homology (KH) domain	Nucleic acid-binding
efhand	EF hand	Calcium-binding
Mito_carr	Mitochondrial carrier protein	Energy transfer in the mitochondrial membrane
HEAT	HEAT repeat	Intracellular transport processes
GTP_EFTU	Elongation factor Tu GTP binding domain	GTP-binding
GTP_EFTU_D2	Elongation factor Tu domain 2	tRNA-binding
HA2	Helicase associated domain (HA2)	Nucleic acid-binding
Histone	Core histone H2A/H2B/H3/H4	DNA-binding
Adaptin_N	Adaptin N terminal region	Interaction with components of the coated vesicles

Figure 8. Distribution of protein domains and families in computationally predicted and experimentally validated pADPr binding proteins. The graph shows the number of occurrences for the 12 most common Pfam domains in (A) putative pADPr binding proteins identified through a 90% similarity sequence search based on the original consensus pADPr binding motif (Supplementary Table S1), (B) a sub-dataset of putative pADPr binding proteins corresponding to the refined pADPr binding module derived from peptides polymer blot analysis (Supplementary Table S2) and (C) pADPr-associated proteins identified by MS in anti-pADPr immunoprecipitation assays in SK-N-SH cells following alkylation-induced DNA damage (Supplementary Table S3).

experimental dataset (Figure 8C). Interestingly, some members of the zf-C₃HC₄ (Ring finger) family are also found with this more stringent motif screen. Ring-finger proteins notably includes Rad 5/Rad 18 (40), BRCA1 (41) and RNF8 (42,43), a group of proteins known to mediate cooperation between ubiquitin-conjugating enzymes in DNA repair, and CHFR, a pADPr binding ubiquitin lyase involved in mitotic stress response (6,44). Another protein domain specifically abundant in the dataset generated with the refined pADPr binding motif is the SNF2_N domain (Figure 8B), which is found in proteins involved in a variety of processes including transcription regulation, DNA repair, DNA recombination and chromatin unwinding. Clearly, the *in silico* protein dataset generated with the refined pADPr binding motif is more closely related to the experimentally generated one. Compared with the dataset generated with the original consensus, both the *in silico* refined motif and the experimental dataset feature a high proportion of protein motifs related to RNA metabolism (RRM_1, Helicase_C, KH_1, DEAD, H2A) and chromatin-remodeling proteins. That strongly suggests that the refined pADPr binding motif dataset is representative of the actual biological diversity of pADPr binding proteins.

From the comparative evaluation of *in silico*-based prediction of pADPr binding proteins and pADPr-associated

proteins found in pADPr immunoprecipitates, one can conclude that both the original and the refined consensus pADPr binding motif are appropriate for the prediction of pADPr binding proteins since both motifs are represented in about the same number of experimentally identified proteins sequences. This can be seen on the Venn diagram displaying the distribution of pADPr binding candidates among the three approaches selected for this study (Figure 9). At first look, it might seem that the number of experimentally validated proteins is low compared with the large number of predicted pADPr binding proteins. However, that statement should be put into context. First, *in silico* analysis only considers primary amino acid sequences; that is, although the use of a consensus sequence for database searching does improve the likelihood of detecting pADPr binding substrates, it does not take into account the structural determinants required for protein-pADPr interaction and hence leads to some false positives. Second, *in silico* predictions are performed over the entire human proteome without considering cell- or tissue-specific protein expression. Third, MS is not able to detect proteins of very low absolute or relative abundance whereas large dynamic range and low protein concentrations do not affect computer-based predictions. Finally, proteins that are part of stable pADPr-containing protein complexes or making strong interactions with

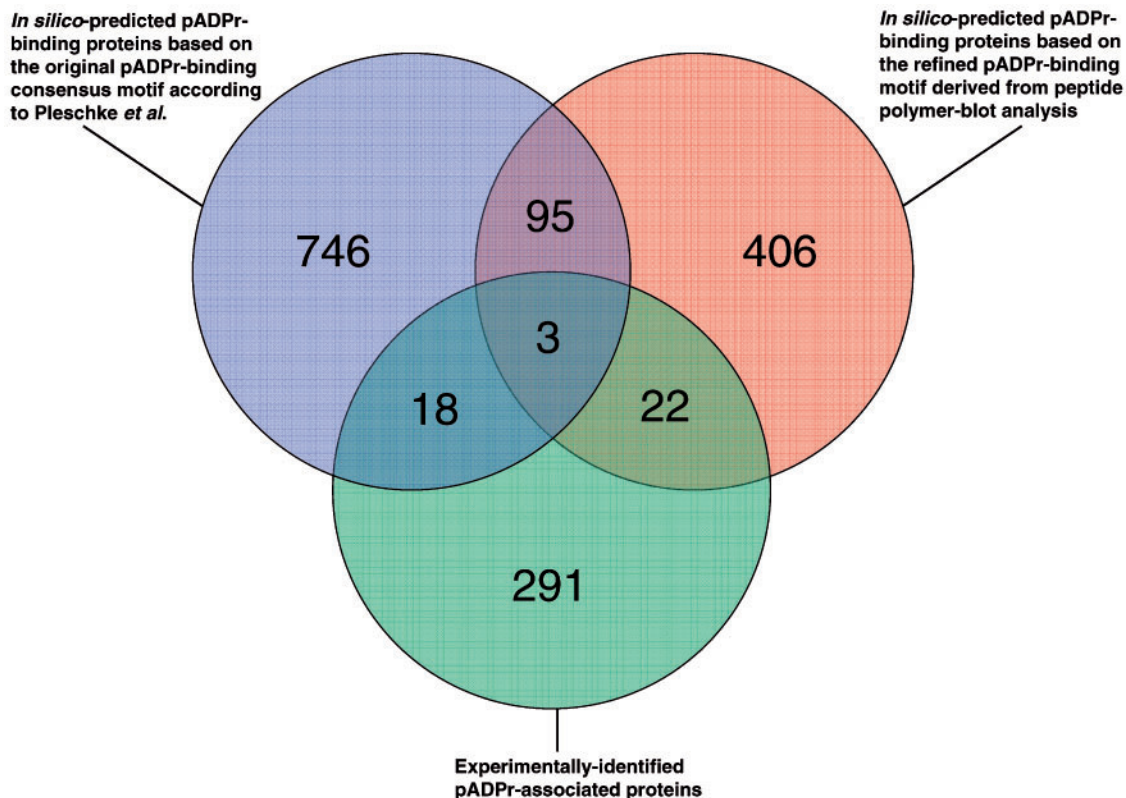


Figure 9. Venn diagram illustrating the overlap between the three pADPr binding candidates datasets described in this study. Overlapping circles shows the distribution of *in silico* predicted proteins revealed through the use of the consensus pADPr binding motif proposed by Pleschke *et al.* (3) and the refined pADPr binding motif derived from sequence alignment of experimentally validated pADPr binding regions from peptide polymer blot analysis. The relationship between the two *in silico* prediction approaches and experimental identification of pADPr-associated proteins in pADPr immunoprecipitates is illustrated as a third intersecting circle.

Table 3. A summary of the major pADPr-regulated pathways

Biological processes	pADPr binding and pADPr-associated proteins	Functions	References
DNA damage signaling and DNA repair	DNA-PK, XRCC1, XRCC5 (Ku86), XRCC6 (Ku70), MSH2, MSH6, DNA damage-binding protein 1 (Xeroderma pigmentosum group E-complementing protein), DNA excision repair protein ERCC-6, BRCA1, DNA repair and recombination protein RAD54-like, hnRNPs, Non-POU domain-containing octamer-binding protein (54 kDa nuclear RNA- and DNA-binding protein (PSF/p54(nrb))), DNA-repair protein complementing XP-C, alkylated DNA repair protein alkB homolog 4, XPA, p53, Mre11, ATM, p21, DNA ligase 3, Aprataxin PNK-like factor (APLF), DNA cross-link repair 1A protein (SMN1)	Detection and early response to DNA strand-breaks, DNA repair	(3,7,45–56)
Modification of chromatin structure	Condensin complex subunit 1 (hCAP-D2/Eg7), SMC2, SMC4, Chromobox protein homolog 1/5, Lamin-A/C, SWI/SNF-related matrix-associated actin-dependent regulator of chromatin subfamily A member 5, Histones, Chromodomain-helicase-DNA-binding protein 1/5	Compaction and decondensation of chromatin	(57–60)
Transcription	Telomerase reverse transcriptase, helicases, chromatin-specific transcription elongation factor FACT 140 kDa subunit, Transcriptional regulator ATRX, transcription intermediary factor 1-beta, probable global transcription activator SNF2L1, transcriptional activator protein Pur-alpha, transcription factor B1 (mitochondrial), activated RNA polymerase II transcription cofactor 4 variant, polymerase I and transcript release factor, Activating signal cointegrator 1 complex subunit 3, DNA-directed RNA polymerase II 140 kDa polypeptide, RUVBL2 protein, EBNA-2 co-activator variant, RHA helicase A, nucleolar RNA helicase 2, U5 snRNP-specific 116 kDa protein, U5 snRNP-specific 200 kDa protein, hnRNPs, DEAD-box RNA helicases p72 (DDX17), transcriptional repressor protein YY1, PARP-9/BAL1, PARP-14/BAL2, PARP-15/BAL3, HMG proteins, transcription factor SPI1, Histone acetyltransferase p300, histone acetyltransferase PCAF	DNA-directed RNA synthesis	(24–26,61–71)
Replication	Helicases, MCM3, MCM4, MCM5, MCM7, DNA primase, DNA topoisomerase, DNA polymerase, replication factor C subunit 4, replication factor C subunit 5, telomerase reverse transcriptase	Synthesis of DNA strands from a parent molecule	(2,72)
RNA metabolism, RNA splicing and protein synthesis	Helicases, hnRNPs, SFQP, splicing factor 3B subunit 3, pre-mRNA-splicing factor SYF1, splicing factor 3B subunit 1, putative pre-mRNA-splicing factor ATP-dependent RNA helicase DHX15, splicing factor, arginine/serine-rich 3, RNA-binding protein PNO1, SF2/ASF-1, pre-mRNA-splicing factor 19, regulator of nonsense transcripts 1, cytoplasmic FMR1-interacting protein 1, nuclease sensitive element-binding protein 1, spliceosome RNA helicase BAT1, mRNA turnover protein 4 homolog, elongation factor 1-alpha 1, elongation factor 2, polyadenylate-binding protein 1	Pre-mRNA processing, transport, localization, mRNA stability	(12,35–38,73–78)
Cell death	AIF, hexokinase-1, HKDC1, cell-division cycle and apoptosis regulator protein 1, deleted in breast cancer gene 1 protein (DBC-1), BID, Caspase-10, prohibitin, Mitochondrial inner membrane protein (mitofilin), DEK, death-associated protein kinase 1/2/3, CAD	Regulation of cell survival, apoptosis	(24,79–85)
Cell-cycle and mitosis	Cell-division cycle and apoptosis regulator protein 1, Cullin-1, Cullin 4A, CDK1 (Cdc2), CDK2, Aurora-A kinase interacting protein, Cenp-A, Cenp-B, Cenp-T, spindle assembly checkpoint protein MAD1, NIMA-related protein kinase Nek10, protein regulator of cytokinesis 1, BUB3, centrosomal protein of 192 kDa, cell-division control protein 6 homolog, cell-division cycle-associated 7-like protein, cell-cycle checkpoint protein RAD17, nucleolar and spindle-associated protein 1, CHFR	Progression through cell-cycle, spindle assembly and structure, cell-cycle checkpoints	(6,86–93)

Selected pADPr binding protein candidates revealed from *in silico* prediction-based or experimental analysis (bold) are proposed for each of the pathways.

proteins that are capable of pADPr binding proteins will not appear in predicted datasets but will likely be identified using experimental approaches. More rigorous studies will be required to improve prediction reliability for pADPr binding proteins and reach a lower rate of false

positive identifications. Even if the protein datasets predicted by the two pADPr binding motifs both share a bias towards nucleic acid metabolism, only 98 proteins are common to both and their limited overlap makes them complementary. On the other side, 43 proteins identified

empirically have a pADPr binding motif. This largely outnumbers any other studies that attempted to determine potential binding partners of pADPr. Moreover, we identified several other pADPr-associated proteins that can either be covalently poly(ADP-ribosyl)ated or noncovalently binders of pADPr without matching a typical pADPr binding motif [e.g. PARP-1, DNA-PK, XRCC5 (Ku86), AIF]. Collectively, these pADPr-associated proteins represent the most comprehensive and detailed information related to pADPr binding reported so far.

DISCUSSION

The experimental demonstration of pADPr binding has traditionally been challenging because of the complexity of interactions between proteins and pADPr, and because of the transient nature of the pADPr-mediated biological response. With technological advances enabling biological questions to be addressed proteome-wide, the entire pADPr interactome is now amenable for scientific investigation. This is particularly useful in the context of poly(ADP-ribosylation), since this phenomenon potentially influences many different cell functions through molecular interactions with numerous pADPr binding substrates (summarized in Table 3).

The greatest advantage of a proteome-wide study like the one presented here lies in the acceleration of the pace at which pADPr binding candidates are discovered compared with traditional approaches. Although these candidates will require additional validation, their disclosure opens up considerable opportunity for new hypothesis-driven experiments.

Our understanding of poly(ADP-ribosylation)-related phenomena should grow more rapidly as studies target proteins with a putative pADPr binding motif, although motif prediction presents difficulties as matches are not strictly conserved. Pattern screening remains a valuable tool to identify interesting targets and their most probable pADPr binding region. This is especially true if one uses our refined pADPr binding motif as it generates a more restricted set of candidates than the original motif and better correlates with experimentally identified pADPr-associated proteins.

We believe that this work represents a valuable investigation into the pADPr interactome and reveals the potential of pADPr to impact a wide range of critical biological functions. By combining bioinformatics-based predictions, pADPr binding peptide blot assays, two-dimensional electrophoresis and large-scale LC-MS/MS identification of immunoprecipitated pADPr-associated proteins, this study represents the first large-scale proteomic identification of pADPr binding proteins and provides insights into the pathways that can be modulated by poly(ADP-ribosylation).

SUPPLEMENTARY DATA

Supplementary data are available at NAR Online.

ACKNOWLEDGEMENTS

We would like to thank Christophe Combet (UMR 5086 CNRS, France) for help with PattInPROT and Pierre Gagné for critical reading of the article. We also thank Joanna M. Hunter for MALDI-TOF MS analysis and Louis M. Nicole for technical help with 2D-gels.

FUNDING

United States Public Health Services and National Institute of Neurological Disorders and Stroke (USPHS NINDS 039148); Canadian Institutes for Health Research (CIHR MOP-14052 and MOP-74648); scholarship from Fonds de la Recherche en Santé du Québec (FRSQ) (to J.P.G.); Strategic Training Program grant in genomics, proteomics and bioinformatics (CIHR STP-53894 to J.P.G.). Funding for open access charge: Canadian Institutes of Health Research (CIHR).

Conflict of interest statement. None declared.

REFERENCES

- Nishizuka, Y., Ueda, K., Honjo, T. and Hayaishi, O. (1968) Enzymic adenosine diphosphate ribosylation of histone and poly adenosine diphosphate ribose synthesis in rat liver nuclei. *J. Biol. Chem.*, **243**, 3765–3767.
- D'Amours, D., Desnoyers, S., D'Silva, I. and Poirier, G.G. (1999) Poly(ADP-ribosylation) reactions in the regulation of nuclear functions. *Biochem. J.*, **342** (Pt 2), 249–268.
- Pleschke, J.M., Kleczkowska, H.E., Strohm, M. and Althaus, F.R. (2000) Poly(ADP-ribose) binds to specific domains in DNA damage checkpoint proteins. *J. Biol. Chem.*, **275**, 40974–40980.
- Karras, G.I., Kustatscher, G., Buhecha, H.R., Allen, M.D., Pugieux, C., Sait, F., Bycroft, M. and Ladurner, A.G. (2005) The macro domain is an ADP-ribose binding module. *EMBO J.*, **24**, 1911–1920.
- Egloff, M.P., Malet, H., Putics, A., Heinonen, M., Dutartre, H., Frangeul, A., Gruez, A., Campanacci, V., Cambillau, C., Ziebuhr, J. *et al.* (2006) Structural and functional basis for ADP-ribose and poly(ADP-ribose) binding by viral macro domains. *J. Virol.*, **80**, 8493–8502.
- Ahel, I., Ahel, D., Matsusaka, T., Clark, A.J., Pines, J., Boulton, S.J. and West, S.C. (2008) Poly(ADP-ribose)-binding zinc finger motifs in DNA repair/checkpoint proteins. *Nature*, **451**, 81–85.
- Fahrer, J., Kranaster, R., Altmeyer, M., Marx, A. and Burkle, A. (2007) Quantitative analysis of the binding affinity of poly(ADP-ribose) to specific binding proteins as a function of chain length. *Nucleic Acids Res.*, **35**, e143.
- Andrabi, S.A., Kim, N.S., Yu, S.W., Wang, H., Koh, D.W., Sasaki, M., Klaus, J.A., Otsuka, T., Zhang, Z., Koehler, R.C. *et al.* (2006) Poly(ADP-ribose) (PAR) polymer is a death signal. *Proc. Natl Acad. Sci. USA*, **103**, 18308–18313.
- Combet, C., Blanchet, C., Geourjon, C. and Deleage, G. (2000) NPS@: network protein sequence analysis. *Trends Biochem. Sci.*, **25**, 147–150.
- O'Farrell, P.H. (1975) High resolution two-dimensional electrophoresis of proteins. *J. Biol. Chem.*, **250**, 4007–4021.
- Mortz, E., Krogh, T.N., Vorum, H. and Gorg, A. (2001) Improved silver staining protocols for high sensitivity protein identification using matrix-assisted laser desorption/ionization-time of flight analysis. *Proteomics*, **1**, 1359–1363.
- Gagne, J.P., Hunter, J.M., Labrecque, B., Chabot, B. and Poirier, G.G. (2003) A proteomic approach to the identification of heterogeneous nuclear ribonucleoproteins as a new family of poly(ADP-ribose)-binding proteins. *Biochem. J.*, **371**, 331–340.
- Menard, L. and Poirier, G.G. (1987) Rapid assay of poly(ADP-ribose) glycohydrolase. *Biochem. Cell Biol.*, **65**, 668–673.

14. Zahradka, P. and Ebisuzaki, K. (1984) Poly(ADP-ribose) polymerase is a zinc metalloenzyme. *Eur. J. Biochem.*, **142**, 503–509.
15. Brochu, G., Duchaine, C., Thibeault, L., Lagueux, J., Shah, G.M. and Poirier, G.G. (1994) Mode of action of poly(ADP-ribose) glycohydrolase. *Biochim. Biophys. Acta*, **1219**, 342–350.
16. Shah, G.M., Poirier, D., Duchaine, C., Brochu, G., Desnoyers, S., Lagueux, J., Verreault, A., Hoflack, J.C., Kirkland, J.B. and Poirier, G.G. (1995) Methods for biochemical study of poly(ADP-ribose) metabolism in vitro and in vivo. *Anal. Biochem.*, **227**, 1–13.
17. Keller, A., Nesvizhskii, A.I., Kolker, E. and Aebersold, R. (2002) Empirical statistical model to estimate the accuracy of peptide identifications made by MS/MS and database search. *Anal. Chem.*, **74**, 5383–5392.
18. Nesvizhskii, A.I., Keller, A., Kolker, E. and Aebersold, R. (2003) A statistical model for identifying proteins by tandem mass spectrometry. *Anal. Chem.*, **75**, 4646–4658.
19. Maere, S., Heymans, K. and Kuiper, M. (2005) BiNGO: a Cytoscape plugin to assess overrepresentation of gene ontology categories in biological networks. *Bioinformatics*, **21**, 3448–3449.
20. Shannon, P., Markiel, A., Ozier, O., Baliga, N.S., Wang, J.T., Ramage, D., Amin, N., Schwikowski, B. and Ideker, T. (2003) Cytoscape: a software environment for integrated models of biomolecular interaction networks. *Genome Res.*, **13**, 2498–2504.
21. Zeeberg, B.R., Feng, W., Wang, G., Wang, M.D., Fojo, A.T., Sunshine, M., Narasimhan, S., Kane, D.W., Reinhold, W.C., Lababidi, S. *et al.* (2003) GoMiner: a resource for biological interpretation of genomic and proteomic data. *Genome Biol.*, **4**, R28.
22. Mulder, N.J., Apweiler, R., Attwood, T.K., Bairoch, A., Bateman, A., Binns, D., Bork, P., Builland, V., Cerutti, L., Copley, R. *et al.* (2007) New developments in the InterPro database. *Nucleic Acids Res.*, **35**, D224–D228.
23. Panzeter, P.L., Zweifel, B., Malanga, M., Waser, S.H., Richard, M. and Althaus, F.R. (1993) Targeting of histone tails by poly(ADP-ribose). *J. Biol. Chem.*, **268**, 17662–17664.
24. Rouleau, M., Aubin, R.A. and Poirier, G.G. (2004) Poly(ADP-ribosyl)ated chromatin domains: access granted. *J. Cell Sci.*, **117**, 815–825.
25. Hassa, P.O., Haenni, S.S., Buerki, C., Meier, N.I., Lane, W.S., Owen, H., Gersbach, M., Imhof, R. and Hottiger, M.O. (2005) Acetylation of poly(ADP-ribose) polymerase-1 by p300/CREB-binding protein regulates coactivation of NF-kappaB-dependent transcription. *J. Biol. Chem.*, **280**, 40450–40464.
26. Haenni, S.S., Hassa, P.O., Altmeyer, M., Fey, M., Imhof, R. and Hottiger, M.O. (2008) Identification of lysines 36 and 37 of PARP-2 as targets for acetylation and auto-ADP-ribosylation. *Int. J. Biochem. Cell Biol.*, **40**, 2274–2283.
27. Kappes, F., Fahrner, J., Khodadoust, M.S., Tabbert, A., Strasser, C., Mor-Vaknin, N., Moreno-Villanueva, M., Burkle, A., Markovitz, D.M. and Ferrando-May, E. (2008) DEK is a poly(ADP-ribose) acceptor in apoptosis and mediates resistance to genotoxic stress. *Mol. Cell. Biol.*, **28**, 3245–3257.
28. Cardenas-Corona, M.E., Jacobson, E.L. and Jacobson, M.K. (1987) Endogenous polymers of ADP-ribose are associated with the nuclear matrix. *J. Biol. Chem.*, **262**, 14863–14866.
29. Cohausz, O., Blenn, C., Malanga, M. and Althaus, F.R. (2008) The roles of poly(ADP-ribose)-metabolizing enzymes in alkylation-induced cell death. *Cell Mol. Life Sci.*, **65**, 644–655.
30. Forsburg, S.L. (2008) The MCM helicase: linking checkpoints to the replication fork. *Biochem. Soc. Trans.*, **36**, 114–119.
31. Chi, N.W. and Lodish, H.F. (2000) Tankyrase is a golgi-associated mitogen-activated protein kinase substrate that interacts with IRAP in GLUT4 vesicles. *J. Biol. Chem.*, **275**, 38437–38444.
32. Sbdio, J.I., Lodish, H.F. and Chi, N.W. (2002) Tankyrase-2 oligomerizes with tankyrase-1 and binds to both TRF1 (telomere-repeat-binding factor 1) and IRAP (insulin-responsive aminopeptidase). *Biochem. J.*, **361**, 451–459.
33. Yeh, T.Y., Sbdio, J.I., Tsun, Z.Y., Luo, B. and Chi, N.W. (2007) Insulin-stimulated exocytosis of GLUT4 is enhanced by IRAP and its partner tankyrase. *Biochem. J.*, **402**, 279–290.
34. Malanga, M., Czubaty, A., Girstun, A., Staron, K. and Althaus, F.R. (2008) Poly(ADP-ribose) binds to the splicing factor ASF/SF2 and regulates its phosphorylation by DNA topoisomerase I. *J. Biol. Chem.*, **283**, 19991–19998.
35. Elkaim, R., Thomassin, H., Niedergang, C., Egly, J.M., Kempf, J. and Mandel, P. (1983) Adenosine diphosphate ribosyltransferase and protein acceptors associated with cytoplasmic free messenger ribonucleoprotein particles. *Biochimie*, **65**, 653–659.
36. Thomassin, H., Martins de Sa, C., Scherrer, K., Maniez, C. and Mandel, P. (1988) Cytoplasmic poly(ADP-ribose) polymerase and poly(ADP-ribose) glycohydrolase in AEV-transformed chicken erythroblasts. *Mol. Biol. Rep.*, **13**, 35–44.
37. Jesser, M., Chypre, C., Hog, F. and Mandel, P. (1993) Cytoplasmic poly(ADP-ribose) polymerase from mouse plasmacytoma free messenger ribonucleoprotein particles: purification and characterization. *Biochem. Biophys. Res. Commun.*, **195**, 558–564.
38. Tanuma, S. and Endo, H. (1990) Purification and characterization of an (ADP-ribose)_n glycohydrolase from human erythrocytes. *Eur. J. Biochem.*, **191**, 57–63.
39. Finn, R.D., Mistry, J., Schuster-Bockler, B., Griffiths-Jones, S., Hollich, V., Lassmann, T., Moxon, S., Marshall, M., Khanna, A., Durbin, R. *et al.* (2006) Pfam: clans, web tools and services. *Nucleic Acids Res.*, **34**, D247–D251.
40. Ulrich, H.D. and Jentsch, S. (2000) Two RING finger proteins mediate cooperation between ubiquitin-conjugating enzymes in DNA repair. *EMBO J.*, **19**, 3388–3397.
41. Starita, L.M. and Parvin, J.D. (2003) The multiple nuclear functions of BRCA1: transcription, ubiquitination and DNA repair. *Curr. Opin. Cell Biol.*, **15**, 345–350.
42. Huen, M.S., Grant, R., Manke, I., Minn, K., Yu, X., Yaffe, M.B. and Chen, J. (2007) RNF8 transduces the DNA-damage signal via histone ubiquitylation and checkpoint protein assembly. *Cell*, **131**, 901–914.
43. Mailand, N., Bekker-Jensen, S., Fastrup, H., Melander, F., Bartek, J., Lukas, C. and Lukas, J. (2007) RNF8 ubiquitylates histones at DNA double-strand breaks and promotes assembly of repair proteins. *Cell*, **131**, 887–900.
44. Chaturvedi, P., Sudakin, V., Bobiak, M.L., Fisher, P.W., Mattern, M.R., Jablonski, S.A., Hurle, M.R., Zhu, Y., Yen, T.J. and Zhou, B.B. (2002) Chfr regulates a mitotic stress pathway through its RING-finger domain with ubiquitin ligase activity. *Cancer Res.*, **62**, 1797–1801.
45. Haince, J.F., McDonald, D., Rodrigue, A., Dery, U., Masson, J.Y., Hendzel, M.J. and Poirier, G.G. (2008) PARP1-dependent kinetics of recruitment of MRE11 and NBS1 proteins to multiple DNA damage sites. *J. Biol. Chem.*, **283**, 1197–1208.
46. Haince, J.F., Kozlov, S., Dawson, V.L., Dawson, T.M., Hendzel, M.J., Lavin, M.F. and Poirier, G.G. (2007) Ataxia telangiectasia mutated (ATM) signaling network is modulated by a novel poly(ADP-ribose)-dependent pathway in the early response to DNA-damaging agents. *J. Biol. Chem.*, **282**, 16441–16453.
47. Malanga, M. and Althaus, F.R. (2005) The role of poly(ADP-ribose) in the DNA damage signaling network. *Biochem. Cell Biol.*, **83**, 354–364.
48. Ruscetti, T., Lehnert, B.E., Halbrook, J., Le Trong, H., Hoekstra, M.F., Chen, D.J. and Peterson, S.R. (1998) Stimulation of the DNA-dependent protein kinase by poly(ADP-ribose) polymerase. *J. Biol. Chem.*, **273**, 14461–14467.
49. Marti, T.M., Kunz, C. and Fleck, O. (2002) DNA mismatch repair and mutation avoidance pathways. *J. Cell. Physiol.*, **191**, 28–41.
50. Wittschieben, B.O. and Wood, R.D. (2003) DDB complexities. *DNA Repair*, **2**, 1065–1069.
51. Shrivastav, M., De Haro, L.P. and Nickoloff, J.A. (2008) Regulation of DNA double-strand break repair pathway choice. *Cell Res.*, **18**, 134–147.
52. Carpenter, B., MacKay, C., Alnabulsi, A., MacKay, M., Telfer, C., Melvin, W.T. and Murray, G.I. (2006) The roles of heterogeneous nuclear ribonucleoproteins in tumour development and progression. *Biochim. Biophys. Acta*, **1765**, 85–100.
53. Bouchard, V.J., Rouleau, M. and Poirier, G.G. (2003) PARP-1, a determinant of cell survival in response to DNA damage. *Exp. Hematol.*, **31**, 446–454.
54. Bladen, C.L., Udayakumar, D., Takeda, Y. and Dynan, W.S. (2005) Identification of the polypyrimidine tract binding protein-associated splicing factor p54(nrb) complex as a candidate DNA double-strand break rejoining factor. *J. Biol. Chem.*, **280**, 5205–5210.
55. El-Khamisy, S.F., Masutani, M., Suzuki, H. and Caldecott, K.W. (2003) A requirement for PARP-1 for the assembly or stability of

